Tailoring high-temperature radiation and the resurrection of the incandescent source

Citation: Ilic, Ognjen; Bermel, Peter; Chen, Gang; Joannopoulos, John D.; Celanovic, Ivan and Soljačić, Marin. "Tailoring High-Temperature Radiation and the Resurrection of the Incandescent Source." Nature Nanotechnology 11, no. 4 (January 2016): 320–324. © 2016 Macmillan Publishers Limited

As Published: http://dx.doi.org/10.1038/nnano.2015.309

Publisher: Nature Publishing Group

Persistent URL: http://hdl.handle.net/1721.1/109242

Version: Original manuscript: author's manuscript prior to formal peer review

Tailoring ultra-high temperature radiation: the resurrection of the incandescent source

Authors: Ognjen Ilic[1]*, Peter Bermel[2], Gang Chen[3], John D. Joannopoulos[1], Ivan Celanovic[1], Marin Soljačić[1]

Affiliations:

[1]Research Laboratory of Electronics, Massachusetts Institute of Technology, Cambridge, Massachusetts 02139, USA.

[2]School of Electrical and Computer Engineering, Birck Nanotechnology Center, Purdue University, West Lafayette, Indiana 47906, USA.

[3]Department of Mechanical Engineering, Massachusetts Institute of Technology, Cambridge, Massachusetts 02139, USA.

*Correspondence to: ilico@mit.edu

Radiation from very hot objects (such as the Sun and incandescent light-bulbs) is of tremendous utility, yet a large fraction of the radiated energy is wasted: for example, in solar cells, the mismatch between the Sun's spectrum and the cell's absorption profile limits efficiency[1]; in incandescent light-bulbs, most of the energy is lost as heat[2]. For moderate temperatures, shaping thermal emission is possible through wavelength-selective radiators such as photonic crystals[3-13]. However, thermal emission tailoring at elevated temperatures (>1000K) remains exceedingly difficult[14-18]. Here, we address this challenge by coupling the hot emitter with a cold-side nanophotonic interference system. In particular, we show that a plain incandescent (3000K) filament, surrounded by an interference system uniquely optimized to reflect infrared and transmit visible light for all angles, becomes a light source that reaches luminous efficiencies close to the limit for lighting applications (~40%), surpassing all existing lighting technologies. In an experimental proof-of-concept, we demonstrate efficiency approaching that of commercial fluorescent or LED bulbs, but with exceptional reproduction of colors and high and scalable power. These results showcase the potential of spectral tailoring and enable a new high-temperature frontier in optics, with applications in thermophotovoltaic energy conversion[3-5] and lighting.

Consider a thermal emitter of emissivity $\epsilon(\lambda,T)$ sandwiched between two identical structures of reflectance $R(\lambda)$ and transmittance $T(\lambda)$, separated by a small gap, as shown in Fig. 1c. In general, the emissivity of a high temperature emitter depends on temperature and wavelength. Such an emitter can be made of uniform, un-patterned, bulk material (e.g. refractory metals such as tungsten or tantalum), but can also be a photonic crystal with wavelength-selective emission properties. Similarly, in the simplest form, the filtering structure is a layered stack of materials of different refractive index, but can also be a 2-dimensional or a 3-dimensional photonic crystal. By tracing the reflected radiation in the cavity surrounding the emitter, we show (see Supplementary Discussion) that the effective emissivity of this emitter-tailoring-structure system can be expressed as

$$\epsilon_{\text{eff}} = \epsilon\left[\frac{FT}{1-F^2R(1-\epsilon)} + \frac{(1-F)(1+FR)}{1-F^2R(1-\epsilon)}\right] \quad (1)$$

where ϵ is the original emissivity of the thermal emitter and F is the view factor characteristic to the geometry. The view factor equals the proportion of the radiation leaving the emitter that is intercepted by the enclosing surface. Expression (1) highlights the potential to tailor thermal emission by designing the surrounding cold-side structure properties. In such a manner, the radiation spectrum of extremely high temperature emitters can be modified without the need for any structural patterning of the emitter surface. The cavity effect due to the surrounding structure results in a portion of the power emitted at unwanted wavelengths to be reabsorbed by the thermal emitter. Applying a similar analysis as before and using Kirchoff's law – at thermal equilibrium, the absorptivity of an object equals its emissivity – allows us to express the fraction of reabsorbed power as $P_r / P_0 = \epsilon^2 F^2 R / (1 - F^2 R(1-\epsilon))$, where P_0 is the original amount of the emitted power (see Supplementary Discussion). This shows that the original spectrum of the

thermal emitter is not just passively filtered, but that the temperature of the emitter itself is tailored by the surrounding photonic structure. Derivations above assume diffusive surfaces and diffusive view factors; in the Supplementary Discussion, we extend our analysis to include specularly reflecting surfaces and show that, in our case, the two methods yield similar results.

We apply this concept to control the thermal emission spectrum of an incandescent filament. As mentioned previously, an incandescent filament is an inefficient source of lighting, as most of the power is emitted at infrared wavelengths, invisible to human eye. Surrounding the filament with interference structures designed to transmit visible and recycle IR light, for a wide range of emission angles, dramatically improves the efficiency. The efficiency of a lighting source (incandescent or otherwise) is defined as the ratio of the total emitted luminous flux and the total supplied power. Because incandescent sources emit essentially all supplied power into radiation, the *luminous* efficiency η can be written as:

$$\eta = \frac{\int_0^\infty P(T,\lambda)V(\lambda)\mathrm{d}\lambda}{\int_0^\infty P(T,\lambda)\mathrm{d}\lambda} \qquad (2)$$

where $P(T,\lambda)$ is the (hemispherical) spectral emissive power of the emitter at temperature T, and $V(\lambda)$ is the photopic luminosity function, which characterizes the spectral sensitivity of the human eye[19]. The luminous efficiency can theoretically assume any value from 0 to 1; lighting sources, however, also need to faithfully reproduce colors. This requires broadband emission throughout the visible spectrum. The index that characterizes the quality of light is known as the color rendering index (CRI); it attains its peak value (100) for high temperature broadband emitters such as incandescent light bulbs (see Supplementary Fig. 3). An excellent lighting source would then be a hypothetical high-temperature black body that emits only at visible

wavelengths. Such an emitter would have a luminous efficiency of at most 40-45% (see Methods).

Figure 1a shows that we can approach such high efficiencies by incorporating one-dimensional photonic films made of commonly-deposited materials, and amenable to large-scale fabrication. The notion of increasing the efficiency of incandescent light bulbs by recycling IR radiation has been previously suggested[20-22]. In contrast, the novelty of our approach is two-fold. First, rejection of light at unwanted wavelengths (and subsequent reabsorption by the emitter) is possible only with interference stacks that operate for a wide range of *both wavelengths and angles* (as our fabricated example demonstrates, see Fig. 3). The challenge in obtaining a structure with similar spectral properties over the complete 0-90° range differs substantially from conventional photonic films that are designed only for a single angle of interest. The fabricated structure in our work has desirable spectral properties over a wide range of angles. Second, the special shape of the thermal emitter enables efficient reabsorption of unwanted radiation, unlike previous designs[20-22] that suffer from sub-optimal probability of reabsorption. The thin and long radiator-like design of the emitter (see Fig. 1C) allows for resistive heating and, at the same time, provides a large amount of surface area to enable efficient coupling of radiation between the emitter and the planar surrounding structure. Furthermore, such planar device configuration is not sensitive to alignment issues that limit reabsorption and is compatible with thermal emitters such as 2D photonic crystals. It is the combination of these two advances that, for the first time, enables thermal emission tailoring to any significant degree.

Here, we assume a planar emitter-tailoring-structure geometry, where the emitter is a plain tungsten filament and the filtering structure is a one-dimensional layered stack of dielectric materials. The tungsten emitter is at a uniform temperature T, and its optical properties are given

by its temperature-dependent emissivity (see Methods). The layered interference stack comprises of oxides of various refractive indices: from the low-index silica (SiO_2) to the high-index titania (TiO_2). To explore the theoretical potential of this scheme, we assume that no radiation leaks to the sides (i.e. near-unity view factor). Instead of separately optimizing interference structure properties against an arbitrary spectral target, we use the knowledge of the effective emissivity of our combined structure (Eq. 1) to perform direct, system-level optimizations of the *total* luminous efficiency (Eq. 2).

We perform this optimization for several different stack designs (Fig 1). An optimized quarter-wave (QW) stack[23] consisting of two materials (SiO_2 and TiO_2) can be effective to a certain extent at suppressing IR radiation, and allows for a higher luminous efficiency relative to the plain incandescent emitter (Fig. 1a, dashed). However, after the first several dozen periods, the quarter-wave stack no longer offers improved efficiency as additional layers are added. Another well-known issue with a QW-stack design is the rejection of additional higher-order bands at $\lambda_0/3$, $\lambda_0/5$, etc., limiting their potential for very-broadband reflection in the IR spectrum and transmission in the visible spectrum. These unwanted reflection bands can be suppressed by rugate-like stacks[24] that feature a sinusoidal optical profile. We leave the specific details of rugate stack design for the Methods section, and note that both 3-material (Fig. 1a, pink) and 4-material (Fig 1a, orange) rugate stacks represent a marked improvement over the QW stack. In particular, when the total number of layers is small, the 4-material design (with its larger unit cell) performs worse than the 3-material design; this is rectified for stacks with more layers. Another implication of the improved efficiency is that a smaller amount of power is needed to heat the thermal emitter to the desired temperature. Figure 1b shows the power consumed by the emitter enclosed between the interference stacks normalized to the power consumed by the plain

emitter at the same temperature (3000K). For optimized designs, this ratio can be lower than 20%.

Using a 4-material rugate structure as a starting point, we show that an extensive numerical optimization scheme (see Methods) results in designs that reach very high luminous efficiency for a reasonable number of layers (Fig. 1a, red). For example, a system where the optimized interference stack consists of 300 layers of 4 materials (SiO_2, Al_2O_3, Ta_2O_5 and TiO_2) reaches very high luminous efficiency (40%), outperforming alternative, commercially available, energy-efficient lighting sources such as fluorescent (7-13%) and LED (5-13%) lamps[25], as well as state-of-art compact LED bulbs (14-15%[26], 29%[27]). The plotted line of optimized structures (red) shows that the increase in luminous efficiency with any additional layer is no worse than linear. However, the complexity of a global optimization problem consisting of hundreds of variables (layers and materials), makes it difficult to speculate on any global optima in the system. As fabrication methods advance and deposition costs go down, stacks with higher number of layers (and materials), as well as 2D and 3D photonic structures that allow for more efficient light filtering will become appealing[6,7,28]. In addition, it is not unlikely that similar or better performing stacks with fewer layers could be designed in the future using some of the more advanced techniques for optical thin film synthesis.

Figure 2 compares the hemispherical (integrated over all angles) spectral emissive power of a plain emitter (bare tungsten) at 3000K with that of the same emitter surrounded by the 300-layer optimized structures from Fig. 1a. For reference, the shaded purple region corresponds to the luminosity function of the human eye. Because we optimized for the total luminous efficiency, the final effective emissivity closely follows the sensitivity profile of the human eye (as seen by

the red line in Fig. 2). As a result, the thermal emitter in this structure reaches its target temperature (3000K) for 1/10 of the original input power (Fig. 1b).

To demonstrate our approach, we design a proof-of-concept version. The interference structure, for simplicity, consists of only two materials (SiO_2 and Ta_2O_5) and 90 layers in total. The design was obtained using the optimization techniques described above; the structure is arranged in a high view-factor geometry. As previously mentioned, the filament's shape is specifically designed to maximize reabsorption (Fig 1c): it is a thin sheet of polished tungsten, laser-machined into a closely-packed, radiator-like structure that maximizes planar surface area while allowing for resistive heating. Figure 2 shows the spectral emissive power (simulation results) of the emitter-tailoring-structure system (blue). We observe a close match to the spectrum of the plain emitter in the visible, and strong suppression of the emission in the IR. This is true for a wide range of wavelengths and angles: the average reflectance of the fabricated structure at 0(45) degrees is 92%(88%) for the 700-2000nm wavelength range. Figure 3 compares the simulated and the measured reflectance of the fabricated stack as a function of angle and wavelength. We observe strong transmission across the visible spectrum and high reflection in the IR, across a wide range of angles. In addition, there is a very good match between the predicted and the measured reflectance (Fig. 3, also Supplementary Fig. 1).

We characterize the performance of our structure by measuring the emitted spectral intensity at 0° and 45° angles and the amount of supplied electrical power. Figure 4 shows the measured and the modelled spectral intensity of the combined emitter-tailoring-structure system (labelled "emitter + stack") normalized to the intensity of the plain emitter that consumes the same amount of power. As expected, we observe an enhancement of emission in the visible spectrum, and

suppression in the IR. To quantify this increase, we calculate the luminous intensity enhancement χ, given by

$$\chi = \frac{\int_0^\infty E_{\text{emitter + stack}}(P_0,\lambda)V(\lambda)\mathrm{d}\lambda}{\int_0^\infty E_{\text{emitter}}(P_0,\lambda)V(\lambda)\mathrm{d}\lambda} \quad (3)$$

where $E(P_0,\lambda)$ is the spectral emitted flux measured by the detector, when the emitter is consuming electrical power P_0 (approximately 135W in the experiment). From Fig. 4, we calculate $\chi = 3.07(2.90)$, at 0°(45°). The estimated view factor from the setup is ~0.95. We note that the calculation of χ involves the direct comparison of the two measured spectra and as such is not sensitive to (nor does it require) the value of temperature. Even though Fig. 4 shows mostly the spectrum in the visible, the spectral enhancement (relative to the bare emitter) in the visible wavelengths already tells us a great deal about the infrared part of the spectrum. When the amount of electrical power is the same, the stronger emission of light in the visible is a direct evidence of the suppression of emission in the infrared, even though emission in the infrared is not measured. We note that the consumed electrical power includes all emissions as well as losses in the device. The very good match between our measurements at different angles and our model (solid and dashed-dot lines in Fig. 4) allows us to evaluate the performance of our system. Matching the consumed power and the view factor to our model, we estimate the luminous efficiency to be about 6.6% (see Methods). This value already approaches some commercially available compact fluorescent (CFL) bulbs and LED lights[25]. One advantage of our scheme is the high quality of color rendering; since the source of the radiation is a blackbody-like emitter, the broadband tailoring ensures faithful reproduction of colors (see photograph in Supplementary Fig. 3), resulting in a CRI of 95 (to calculate this number we followed 29). For comparison, compact (linear) fluorescent bulbs have CRI of 65-88 (50-90), while the majority of LED

fixtures belong in the 70-90 range[25]. Another important advantage of our scheme is scalability: while LED lights have so far been limited in the total amount of light they can produce[30], high temperature thermal emitters allow for very high luminous flux output, particularly relative to the size of the fixture.

The demonstrated method of tailoring high temperature thermal radiation is scalable and can also be implemented in more compact geometries. However, we would like to emphasize that this work demonstrates a concept that is much more general than efficient lighting. For example, the ability to tailor thermal emission (e.g. to better match the absorption profile of a photovoltaic cell) would have dramatic implications on the performance of solid-state thermophotovoltaic energy conversion schemes[3-5], extending the technological importance of high-temperature thermal emission tailoring. In addition, this concept does not apply just to thermal emitters but to thermal radiation *absorbers* as well. For example, a similar approach can be implemented in a selective absorber element that efficiently captures solar energy to be delivered to the solar cell, but significantly reduces the usually wasted radiation emitted back towards the Sun[4]. Because the high temperature emitter is a plain, un-patterned material, it can withstand extremely high temperatures without structural surface degradation. At temperatures required for efficient incandescent lighting, however, material evaporation from the surface of the emitter may affect the optical properties of the close-by interference structure. This can be particularly pronounced for pure metals such as tungsten (our case) or tantalum, but efforts that include filament doping, introduction of halogen elements and high molecular weight inert gases would reduce this effect. On the other hand, at temperatures needed for thermophotovoltaic energy conversion (such as selective radiators/absorbers[3-5]) of 1500-2000K – still very challenging for direct (hot-side) patterning of the thermal emitter surface – such evaporation effects are drastically reduced. Our

analysis can be extended to include interference structures other than 1D-layered stacks, such as 2D or 3D photonic structures, as well as wavelength-selective emitters. Finally, our results show that these composite systems provide control over the fundamental structural properties of thermal emission and absorption: the designs that we describe here are examples to showcase the immense potential of nanophotonics for tailoring high temperature thermal radiation.

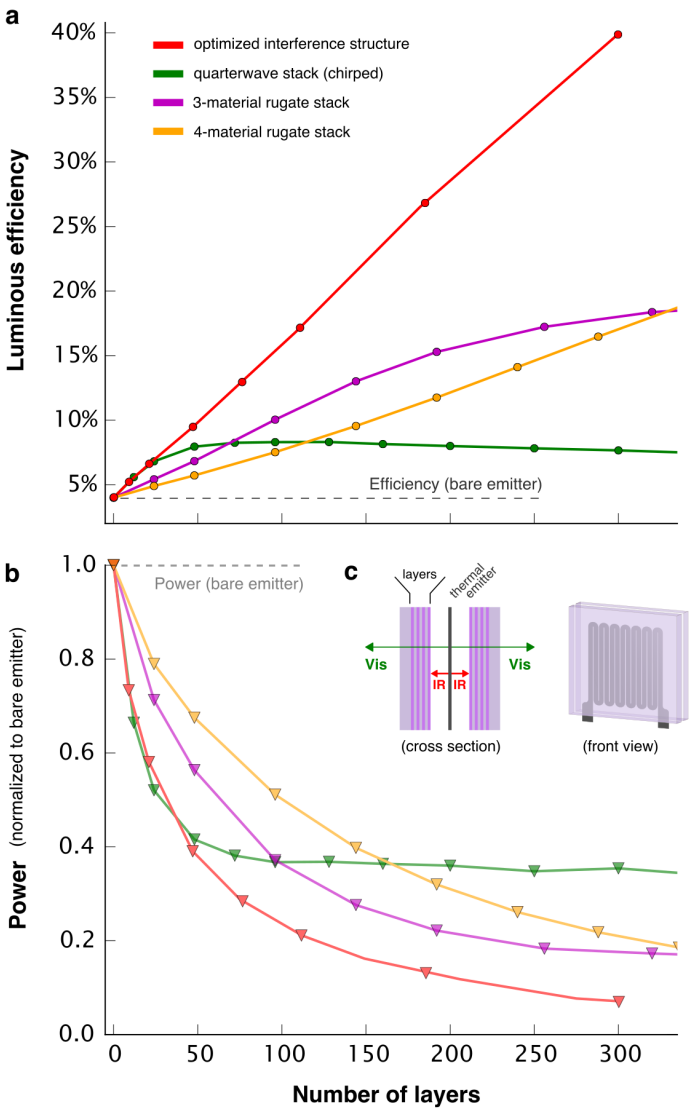

Figure 1 | Potential of cold-side thermal emission tailoring. a, Projected luminous efficiency of a tungsten thermal emitter (3000K) optimally enclosed by interference structures of different design: quarterwave stack (green), 3- and 4- material rugate stack (purple, orange), and stacks designed using a combination of optimization techniques (red; see main text). For quarterwave and rugate stacks, we introduce chirp to increase the bandwidth, and for each number of layers (x-axis) we explore the complete parameter space to find the optimal design (Methods). For all designs, the material refractive indices are bounded by SiO_2 (low) and TiO_2 (high). In addition to these two indices, the designs in red also use intermediate values (e.g. Al_2O_3 and Ta_2O_5). **b**, The amount of power needed for the emitter to reach the temperature of 3000K when it is surrounded by the corresponding designs shown in (**a**). The power is normalized to the power needed to heat the plain emitter to the same temperature (dashed line). **c**, Sketch of the proposed scheme to tailor the thermal emission of high temperature objects. In the case of efficient lighting, we design the surrounding structures to transmit visible and reflect (and thus recycle) IR light for a broad range of wavelengths and angles. Right: sketch of our experimental setup (see Supplementary Fig. 2).

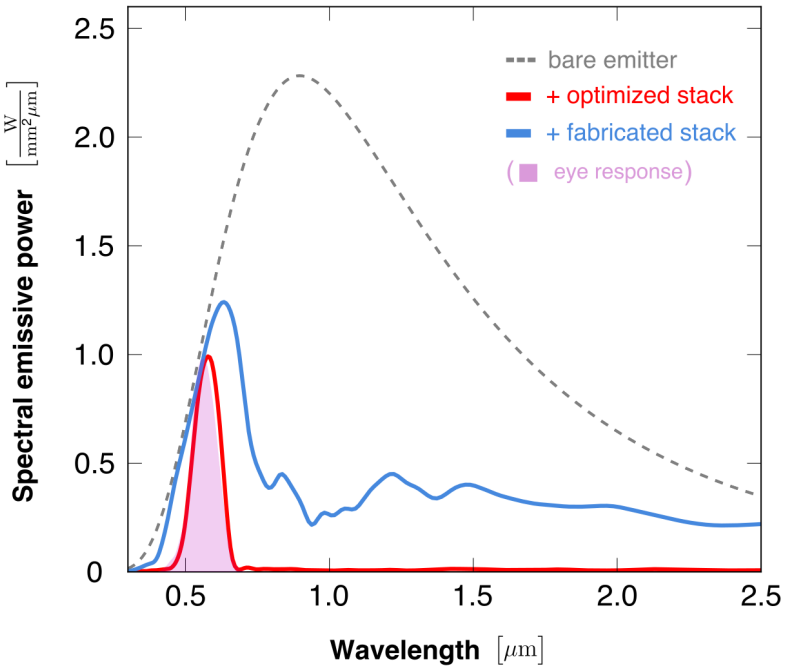

Figure 2 | Effective emissivity of an optimally enclosed structure. The spectral emissive power (calculated) for an emitter (3000K) that is plain tungsten (dashed) or tungsten sandwiched by interference structures (solid; red and blue). The power is integrated over all angles (hemispherical emission). The sensitivity of the human eye (luminosity function[19]) is shown in shaded purple (arbitrary normalization). The optimized structure corresponds to the 300-layer design from Fig. 1a (red); its effective emissivity closely follows the sensitivity profile of the human eye. For simplicity, the fabricated design (blue), consists of 90 layers and only two materials (SiO_2 and Ta_2O_5). It closely matches the spectrum of the plain emitter in the visible and offers strong suppression of emission in the IR.

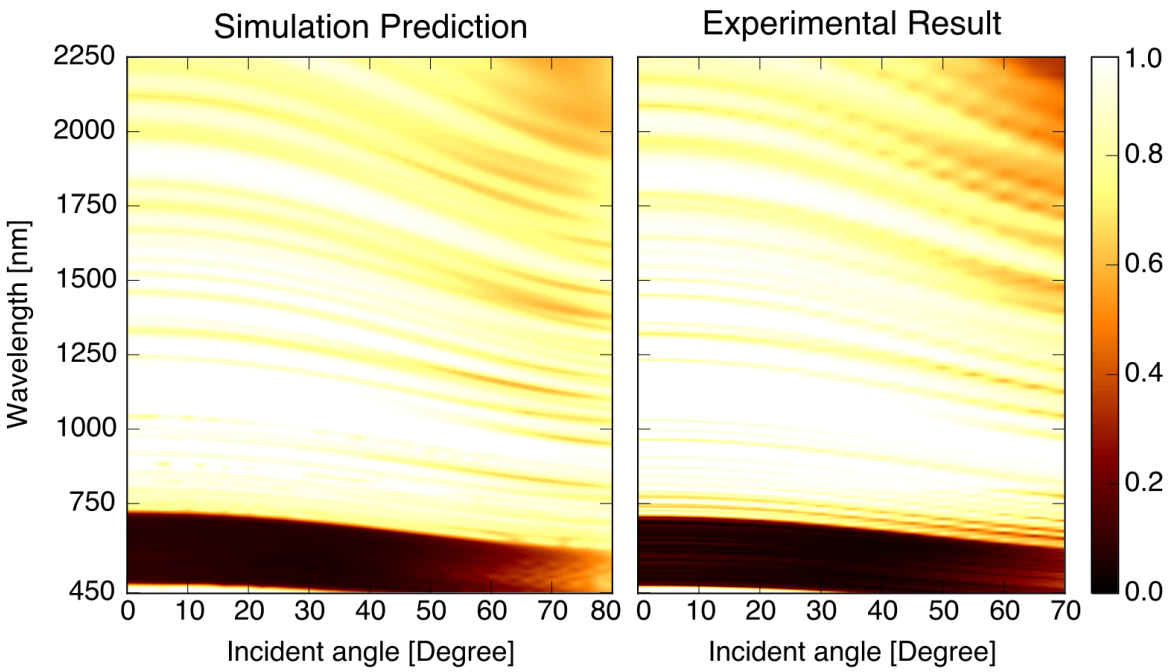

Figure 3 | Simulation and experimental measurements over very wide ranges of wavelength and angle. Comparison between the simulated (left) and measured (right) reflectance spectra of the fabricated 90-layer interference structure (Fig. 2, blue line). In contrast to conventional photonic films designed for a single angle of interest, the challenge is to produce similar spectral properties over a very wide range of angles. The stack shows high transmission across the visible spectrum and high reflection in the IR. The experimental data were restricted to 70 degrees because of the sample size.

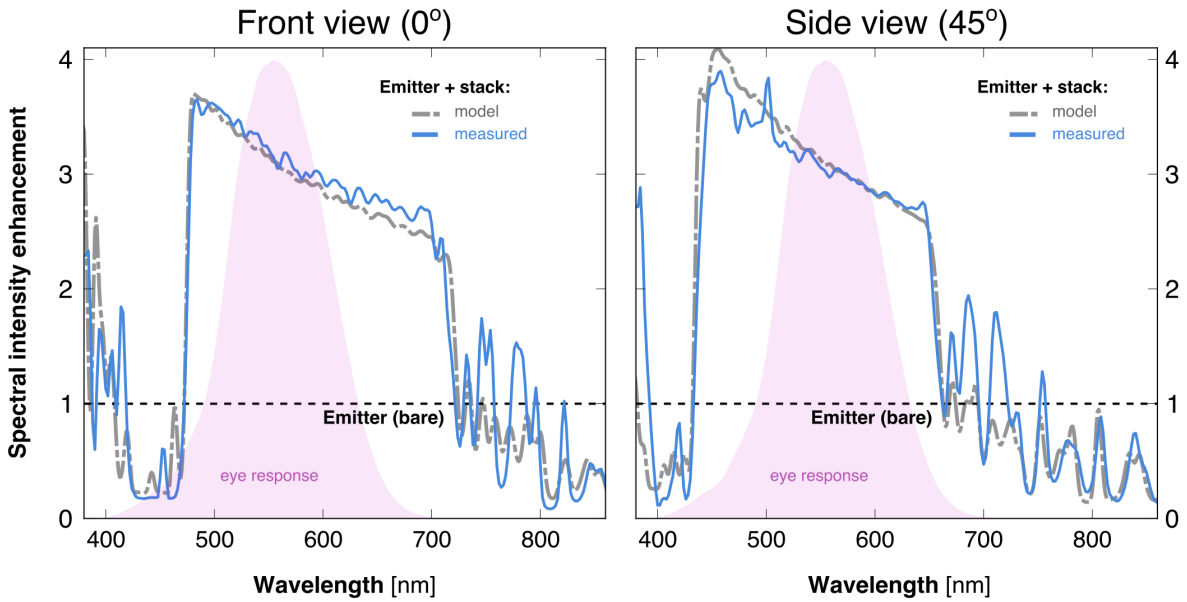

Figure 4 | Experimental demonstration of thermal emission tailoring. Measured (blue, solid) and modelled (gray, dashed-dot) spectral intensity of the combined emitter-tailoring-structure system (labelled "Emitter + stack") normalized to the intensity of the plain emitter (black, dashed) that consumes the same amount of power. The fabricated structure consists of 90 layers (Fig. 3), made of two materials (SiO_2 and Ta_2O_5), deposited on a silica substrate. The spectrum is measured at 0° (front view) and 45° (side view). The sensitivity of the human eye (luminosity function) is shown in shaded purple (arbitrary normalization). For the same amount of input power, we measure a luminous flux that is 3.07(2.90) times enhanced at 0°(45°) compared to that of a plain emitter.

Methods

Ideal luminous efficiency for lighting applications. Using equation (2) from the main text, we can estimate the luminous efficiency of an ideal lighting source. A black (or grey) body at temperature 2800K(5800K), with its spectrum truncated to wavelengths where the luminosity function is ≥1% of its peak value, has a luminous efficiency of 41.9(41.5)%.

Thermal emitter properties and experimental setup details. The thermal emitter is a sheet of refractory metal (tungsten sheet, 80-85μm thick, obtained from H.C. Starck), laser machined into a geometry that allows for both resistive heating as well as efficient reabsorption of reflected light (Supplementary Fig. 2b). Prior to laser cutting, the sheet of tungsten is covered with a thin layer (~10μm) of UV-curable, water-soluble, polymer (DaeCoat^{TM} PCA-120713) to protect against material ablation. Afterwards, the coating is removed in de-ionized water by sonication. Optical properties of refractory metals strongly depend on temperature as well as sample purity and preparation conditions. Supplementary Fig. 4a shows the general dependence of tungsten emittance (normal) on wavelength[31]. The crossover point, in the 1-1.5μm region, separates the spectral regions where the emissivity increases/decreases with temperature.

In our calculations, we use tabulated data for normal spectral emittance[31], in 200K steps for a range of temperatures (1600-3100K). Emittance for angles other than zero is calculated as follows: high temperature dielectric permittivity for tungsten is obtained by fitting the emittance data at each temperature to a sum of Drude-Lorentzian dielectric functions. Once the permittivity (as a function of wavelength and temperature) is known, angular dependence of absorptivity is derived from Fresnel reflection coefficients. Finally, from Kirchoff's law, the (directional,

spectral) emissivity equals the (directional, spectral) absorptivity. For intermediate temperature (temperatures in between the 200K steps), we obtain the emissivity by linear interpolation.

Light emitted by the resistively heated tungsten filament is captured by two detectors, at 0° and 45° angles with respect to the surface of the filament emitter (Supplementary Fig. 2a). The detectors are calibrated to correct for any nonlinearity in the measured signal. The air in the setup is evacuated (P~10^{-6} torr) and argon is added (P~10^{-4} torr). The one-dimensional photonic film was fabricated using ion-beam sputtering at Evaporated Coatings, Inc., with layers of Ta_2O_5 and SiO_2 on a fused-silica substrate (2cm x 2cm). Coatings deposited using ion-beam sputtering have particularly low absorption in the visible and the near-IR: the extinction coefficient for Ta_2O_5 is estimated to be $<10^{-4}$ (550nm, [32]), and the tantala/silica coatings are used for antireflection coatings in precise gravitational wave detectors, with absorption loss on the order of ppm (1064nm, Table 10.1 in [33]). For wavelengths in the mid-IR (>4μm), these materials become absorptive: however, we note from Fig. 2 that a 3000K tungsten emitter radiates a very small fraction of light (~3.8%) in the spectrum above 4μm. Undesired absorption in the optically-thick silica substrate may be further reduced in glasses with particularly low IR-absorption such as Corning's 7979 or Heraeus' Infrasil (in addition, the substrate thickness can be further reduced).

Thermal emitter temperature estimation. Supplementary Figure 4b shows the dependence of tungsten resistivity on temperature[34]. The knowledge of resistivity, together with the shape and size of the emitter, allows us to estimate the temperature from the measured resistance. First, we perform a finite-element heat transfer analysis (COMSOL Multiphysics) to obtain the equilibrium temperature distribution of the emitter, shown in Supplementary Fig. 4c. We observe that only the main part of the emitter (the radiator-like structure) reaches very high temperatures.

Further analysis confirms that most of the power is indeed dissipated in this part of the emitter. In addition, we observe a highly uniform temperature distribution between the central strips of the emitter. Values of high temperature thermal conductivity and heat capacity of tungsten are obtained from literature[35,36].

The measured resistance of the emitter in Fig. 4 of the main text is R=2.90Ω when the interference structure surrounds the emitter, and R=2.62Ω when there is not such structure (plain emitter). In both cases, the measured power delivered to the emitter is the same (135W). Taking into account the uncertainty and the variation in the emitter thickness (80-85μm), these values of resistance imply (based on the resistivity dependence shown in Supplementary Fig. 4b) a temperature estimate for the central part of the emitter of 2900-3050K for the case when the filtering structure is present, and an estimate of 2700-2830K when the emitter is bare. Another way to estimate the temperature is to evaluate the energy of the emitted light, assuming the literature value of temperature-dependent tungsten emittance[31]. It is important to note that at high temperatures, resistivity and, particularly, emissivity data for refractory metals is heavily dependent on the sample preparation process, presence of impurities and surface finish[31,34], which means that the margin of error for our estimates may be significant. With that in mind, our model estimates (given the area of the emitter and the view-factor ~0.95) that to consume 135W of power, the emitter would have a temperature of 2950K, and the total luminous efficiency of the system would be 6.6%.

Interference structure design and optimization. For the custom optimization (Figs. 1&2, red; Fig. 2, blue), we use rugate-like designs (see below) as a starting point, and apply other optimization methods[37], including the needle optimization[38]. Specifically, we use a combination

of local, gradient-based, optimization algorithms[39], made possible by implementing a transfer matrix approach that in addition to calculating luminous efficiency also calculates the necessary derivatives of the efficiency (with respect to each layer thickness) at a comparatively small computational cost. This is combined with a parallelized (MPI) implementation of the calculation that efficiently determines where a new layer should be introduced or an existing layer removed to maximize the figure of merit (lum. efficiency) of the combined system (emitter + stack). The combination of these methods yields the designs with luminous efficiency values plotted in Figures 1 and 2 of the main text.

The purpose of a rugate-like interference structure[24,40] is to suppress the higher-order reflection bands (which for a QW stack designed for wavelength λ_0 occur at $\lambda_0/3$, $\lambda_0/5$, $\lambda_0/7$, etc.), and thus allow for a wide rejection band in the IR (~0.7-2.5μm) while maintaining low reflection in the visible spectrum. This is achieved through a sinusoidal refractive index profile. There are several ways to implement such a profile: for example, the index of refraction *n(x)* or the dielectric permittivity $n^2(x)$ can be sinusoidally dependent on the structure optical thickness *x*. However, it can be shown that the most complete suppression of the reflectance bands at higher harmonics is achieved when the natural logarithm of the refractive index exhibits the sinusoidal profile[40]. Such a structure would have a refractive index profile that satisfies $\ln(n(x)) = a\cos(4\pi x/\lambda_0) + b$, where λ_0 is the design wavelength, and *x* is the optical thickness. The coefficients *a,b* ensure the correct limit to the optical profile and are given by $a = 1/2\ln(n_L/n_H)$ and $b = 1/2\ln(n_L n_H)$ where n_L and n_H denote the low and the high refractive indices.

In practice, the rugate filter profile is obtained by using a discrete set of materials with refractive indices bounded by n_L and n_H (corresponding to SiO_2 and TiO_2 in our case). For a 4-

material rugate structure, the corresponding stacking of layers is [ABCDDCBA], where by definition $n(A)=n_L$, $n(D)=n_H$, and the optical thickness of each layer is $\lambda_0/4$. We increase the bandwidth of our interference structure by introducing period chirping, defined as $T_i = T_{i-1}(1+\varsigma/1-\varsigma)^{1/(N_p-1)}$ where T_i denotes the optical thickness of the i-th period, N_p is the total number of layer periods, and ς is the dimensionless chirp parameter. Given the definitions above, for the QW stack and the 3- and 4- material rugate structure designs from Fig. 1 of the main text, we sweep the complete parameter space to find the optimal rugate design for a given number of layers.

References:

1. Shockley, W. & Queisser, H. J. Detailed balance limit of efficiency of p-n junction solar cells. *J. Appl. Phys.* **32**, 510 (1961).
2. U.S. Department of Energy, Office of Energy Efficiency and Renewable Energy, *2010 U.S. Lighting Market Characterization*, (prepared by Navigant Consulting, Inc., Washington, D.C., 2012).
3. Lin, S. Y., Moreno, J. & Fleming, J. G. Three-dimensional photonic-crystal emitter for thermal photovoltaic power generation. *Appl. Phys. Lett.* **83**, 380 (2003).
4. Lenert, A. *et al*. A nanophotonic solar thermophotovoltaic device. *Nature Nanotechnol.* **9**, 126130 (2014).
5. Chan, W. R. *et al.* Toward high-energy-density, high-efficiency, and moderate-temperature chip-scale thermophotovoltaic. *Proc. Natl. Acad. Sci. U.S.A.* **110**, 53095314 (2013).
6. Greffet, J.-J. *et al.* Coherent emission of light by thermal sources. *Nature* **416**, 1 (2002).
7. Fleming, J. G., Lin, S. Y., El-Kady, I., Biswas, R. & Ho, K. M. All-metallic three-dimensional photonic crystals with a large infrared bandgap. *Nature* **417**, 52 (2002).
8. De Zoysa, M. *et al.* Conversion of broadband to narrowband thermal emission through energy recycling. *Nature Photon.* **6**, 535539 (2012).

9. Raman, A. P., Anoma, M. A., Zhu, L., Rephaeli, E. & Fan, S. Passive radiative cooling below ambient air temperature under direct sunlight. *Nature* **515**, 7528 (2014).
10. Inoue, T., De Zoysa, M., Asano, T. & Noda, S. Realization of dynamic thermal emission control. *Nature Mater.* **13**, 928931 (2014).
11. Liu, X. *et al.* Taming the blackbody with infrared metamaterials as selective thermal emitters. *Phys. Rev. Lett.* **107** (2011).
12. Arpin, K. A. *et al.* Three-dimensional self-assembled photonic crystals with high temperature stability for thermal emission modification. *Nature Commun.* **4**, 2630 (2013).
13. Yu, Z. *et al.* Enhancing far-field thermal emission with thermal extraction. *Nature Commun.* **4**, 1730 (2013).
14. Schlemmer, C., Aschaber, J., Boerner, V. & Luther, J. Thermal stability of micro-structured selective tungsten emitters. *AIP Conf. Proc.* **653**, 164 (2003).
15. Sai, H., Kanamori, Y. & Yugami, H. High-temperature resistive surface grating for spectral control of thermal radiation. *Appl. Phys. Lett.* **82**, 1685 (2003).
16. Nagpal, P. *et al.* Fabrication of carbon/refractory metal nanocomposites as thermally stable metallic photonic crystals. *J. Mater. Chem.* **21**, 10836 (2011).
17. Arpin, K. A., Losego, M. D. & Braun, P. V. Electrodeposited 3D tungsten photonic crystals with enhanced thermal stability. *Chem. Mater.* **23**, 47834788 (2011).
18. Rinnerbauer, V. *et al.* High-temperature stability and selective thermal emission of polycrystalline tantalum photonic crystals. *Opt. Express* **21**, 11482 (2013).
19. Sharpe, L. T., Stockman, A., Jagla, W. & Jagle, H. A luminous efficiency function, $V^*(\lambda)$, for daylight adaptation. *J. Vision* **5**, 3 (2005).
20. Kostlin, H. & Almer, F. H. R. U.S. Patent No. 4017758 (1977).
21. Goldstein, I. S., Fontana, R. P., Thorington, L. & Howson, R. P. The design, construction and performance of an incandescent light source with a transparent heat mirror. *Lighting Res. Technol.* **18**, 93 (1986).
22. Bergman, R. S. Halogen-IR lamp development: a system approach. *J. Illum. Eng. Soc.* **20**, 10 (1991).
23. Hecht, E. *Optics* 4th ed. (Addison-Wesley, San Francisco, 2002).
24. Baumeister, P. Simulation of a rugate filter via a stepped-index dielectric multilayer. *Appl. Optics* **25**, 2644 (1986).

25. U.S. Department of Energy, *Lighting basics*, http://energy.gov/eere/energybasics/articles/lighting-basics, retrieved May 2015.

26. *Next Generation Luminaires™ (NGL) Solid-State Lighting Design Competition*, (2014), sponsored by the U.S. Department of Energy, http://www.ngldc.org.

27. "Philips creates the world's most energy-efficient warm white LED lamp", Press release (April 2013), http://www.newscenter.philips.com/main/standard/news/press/2013/20130411-philips-creates-the-world-s-most-energy-efficient-warm-white-led-lamp.wpd.

28. Lin, S. Y. *et al.* A three-dimensional photonic crystal operating at infrared wavelengths. *Nature* **394**, 251 (1998).

29. Aldrich, M. Dynamic solid state lighting. Thesis, Massachusetts Institute of Technology (2010).

30. U.S. Department of Energy, Office of Energy Efficiency and Renewable Energy, *CALIPER Snapshot Reports (2014)*, http://energy.gov/eere/ssl/caliper-snapshot-reports, retrieved April 2015.

References (Methods)

31. Touloukian, Y. S. & DeWitt, D. P. Thermal radiative properties: metallic elements and alloys, vol. 7., Thermophysical properties of matter (IFI/Plenum, New York, 1970).

32. H. Demiryont, J. R. Sites, and K. Geib. Effects of oxygen content on the optical properties of tantalum oxide films deposited by ion-beam sputtering. *Applied Optics*, **24**, 4, 490, 1985.

33. Harry, G., Bodiya, T.P. & DeSalvo, R. Optical Coatings and Thermal Noise in Precision Measurement (Cambridge University Press, 2012).

34. Desai, P. D., Chu, T. K., James, H. M. & Ho, C. Y. Electrical resistivity of selected elements. *J. Phys. Chem. Ref. Data*, **13**, 1069 (1984).

35. Powell, R. W., Ho, C. Y. & Liley, P. E. Thermal conductivity of selected materials. (National Standard Reference Data Series, National Bureau of Standards, **8**, 1966).

36. White, G. K. & Collocott, S. J. Heat capacity of reference materials: Cu and W. *J. Phys. Chem. Ref. Data* **13**, 1251 (1984).

37. Larouche, S. & Martinu, L. OpenFilters: open-source software for the design, optimization, and synthesis of optical filters. *Appl. Optics* **47**, C219 (2008).
38. Tikhonravov, A. V., Trubetskov, M. K. & DeBell, G. W. Application of the needle optimization technique to the design of optical coatings. *Appl. Optics* **35**, 5493 (1996).
39. Johnson, S. G. The NLopt nonlinear-optimization package, http://ab-initio.mit.edu/nlopt.
40. Carniglia, C. K. A comparison of various rugate filter designs. *Laser-Induced Damage in Optical Materials: 1987*, 2722726 (1988).

Acknowledgments: We thank Paola Rebusco for critical reading and editing of the manuscript, Jay J Senkevich, Walker Chan, Imbert Wang, Aviv Cukierman, Michael Harradon, Ahmet Musabeyoglu, Steven Johnson and Yi Xiang Yeng for valuable discussion. This work was partially supported by the Army Research Office through the ISN under Contract Nos.W911NF-13-D0001. The fabrication part of the effort was supported by the S3TEC, an Energy Frontier Research Center funded by the U.S. Department of Energy (DOE), Office of Science, Basic Energy Sciences (BES), under Award # DE-SC0001299 / DE-FG02-09ER46577.

Author Contributions: All authors contributed to the idea of this study. O.I. and P.B. performed numerical simulations and built the experimental setup. O.I. conducted the measurement and analysis. M.S. supervised the project. O.I., J.D.J. and M.S. wrote the paper with input from all authors.